scientific reports

Check for updates

OPEN

Design and fabrication of a Wilkinson power divider with harmonic suppression for LTE and GSM applications

Gholamhosein Moloudian[1], Sepehr Soltani[2], Sirous Bahrami[3], John L. Buckley[1], Brendan O'Flynn[1] & Ali Lalbakhsh[4]✉

Conventional Wilkinson power dividers (WPDs) can provide acceptable performance close to the nominal center frequency. However, these WPDs can also exhibit poor out-of-band performance while requiring a large footprint. In order to improve on the current state of the art, a modified microstrip WPD is proposed that exhibits a substantially improved stopband and high isolation. A lowpass filter (LPF) structure is utilized in both branches of the power divider to provide harmonic suppression. According to the obtained results, the input return loss ($|S_{11}|$), output return loss ($|S_{22}|$), output insertion loss ($|S_{21}|$) and isolation ($|S_{32}|$) are better than 34.2 dB, 26.2 dB, 3.52 dB and 31.2 dB, respectively. The proposed modified WPD has a wide 20 dB stopband (from 2.54 GHz to 13.48 GHz) and filters the second to seventh harmonics with attenuation levels of greater than 20 dB. The proposed WPD has a small size of 33.8 mm × 27 mm (0.42 λg × 0.33 λg), where λg is the guided wavelength at the operating frequency of 1.8 GHz. The WPD has been fabricated and tested and shows good agreement between simulated and measured results and the proposed design has desirable characteristics for LTE and GSM applications.

In recent years, modern wireless communication systems have become increasingly important, and the demand for high-performance active and passive RF/Microwave components such as antennas[1–3], filters[4–15], power dividers[16–32], mixers[33] and multiplexers[34–38] has grown substantially. In particular, passive microstrip devices such as filters and power dividers have critical specification requirements. These specification requirements include low insertion loss (IL), sharp filter response, also known as high roll-off rate (ROR), compact size, high selectivity, high isolation between output ports, wide stopband response, high suppression factor (SF), simple structure and affordable manufacturing processes. Microwave components which exhibit these attributes play a crucial role in such modern systems.

Microstrip filters such as bandpass filters (BPFs)[4,5] and lowpass filters (LPFs)[6–15] have a key role in the design of modern communication systems as they are used for removing unwanted signals and harmonics from radio signals. In[4], a BPF with compact size and low IL designed using coupled line resonators and spoof surface plasmon resonators for communication applications was presented. Also, recent challenges and techniques for designing BPF were reported in[5]. Moreover, in state-of-the-art wireless communication circuits, RF signal detectors play an essential role in detecting or demodulating any desirable signals from a modulated signal. A compact tunable LPF with sharp ROR and high selectivity for controlling suppression levels and removing unwanted harmonics for use in envelop detector structures was designed and is described in[6]. In addition, in recent years, various techniques and methods such as microstrip stubs[7,8], defected ground structure (DGS)[3,9,10] and T-shaped resonators[11,12] have been utilised for designing LPF structures and microstrip devices.

Indeed, in[3], a high-sensitivity microstrip patch sensor antenna is proposed which uses a DGS technology envisaged for permittivity characterisation. A LPF with wide stopband and low IL using modified T-shaped hairpin resonators has been presented in[12]. Moreover, a compact LPF with sharp ROR and wide stopband using a stepped impedance resonator is proposed in[13,14]. In addition, in[14], an ultra-wide stopband LPF with low IL (less than 0.5 dB) using three-stepped impedance stubs and multiple transmission zeros was reported. Although a

[1]Tyndall National Institute, University College Cork, Cork T12R5CP, Ireland. [2]School of Electrical Engineering, Shiraz University, Shiraz, Iran. [3]Department of Electrical Engineering, Pohang University of Science and Technology, Pohang, South Korea. [4]Macquarie University College, Macquarie University, Sydney, NSW 2109, Australia. ✉email: ali.lalbakhsh@mq.edu.au

compact LPF presenting a good response in terms of a sharp ROR, wide stopband and low IL is presented in[15], the structure is comparatively complex. Combiners, couplers and power dividers are three microstrip passive devices which can be considered essential in modern wireless communication systems for the distribution and processing of RF energy. The Gysel power divider[16,17] and Wilkinson power divider (WPD)[18–32] are very common and useful in RF/microwave communication circuits to divide an input signal into two equal phase output signals, or to combine two equal-phase signals into a combined signal with a 180° phase shift. Based on rapid developments in state-of-the-art communications, the demand for multi band frequency components has increased dramatically in recent years[18,19]. However, conventional WPDs have a large footprint, and small stopband bandwidth requiring additional measures such as coupled-line[20,21], integrating filters and suppression cells[21–32] to mitigate these issues. A wideband BPF power divider with a suppression cell using microstrip stubs and coupled lines was presented in[21,24]. In recent years, several techniques such as microstrip stubs[22,23,25], microstrip electromagnetic bandgap elements[26], bent stub and rectangular resonator[27], asymmetric spiral DGS[28], high-low impedance resonators[29], SMD inductors and resistors[30] and radial open stubs[31,32] have been utilised for designing harmonic suppression structures. In modern communication systems, the demand for multiplexer and multi-port components such as power dividers[16–32] and diplexers[34–38] has been growing rapidly. In addition, designing LPF, BPF and tunable microstrip devices based on LC circuits and analytical methods in[34–38] can be very useful. Also, all LPF and BPF parameters such as ROR, SF, normalised circuit size (NCS), figure of merit (FOM), relative stopband (RSB), tuning range (TR), cut-off frequency (f_c) and center frequency (f_0) are reported in[34,35,38]. The design of a WPD that offers harmonic suppression, compact size, wide stopband performance, sharp ROR, high SF, low-cost implementation, with high isolation between output ports, still remains a challenge at the present time.

In this paper, a WPD with a modified structure is proposed in "Power divider structure design". The design steps associated with the proposed modified WPD is shown in Fig. 1. The presented WPD is designed according to desirable characteristic constraints such as size reduction, high isolation, sharp ROR and wide stopband performance. The design uses LPF structures that are integrated into both branches of a conventional power divider. The remainder of the paper is organised as follows: Designing of the third-order LC circuit, basic and modified resonators, harmonic suppression cells and LPF structure are presented in "LPF design methodology". Conventional and modified WPD and odd and even modes of the proposed WPD are discussed in "Power divider structure design". Discussion of simulation and measurement results, novelty and advantages of the proposed WPD are explained in "Discussion of results and contributions". Finally, "Conclusion" presents a conclusion of this work.

LPF design methodology

The LPF design methodology is depicted in Fig. 1. As seen in the Figure, as a first step, a basic LC resonator is designed based on normalization coefficients of the third-order LPF circuit followed by a microstrip transmission line implementation derived from a detailed mathematical analysis (Fig. 2). In the second step, a design methodology for the modified resonator is presented. One of the important performance parameters for a filter is the roll-off-rate (ROR) which depicts the changing attenuation rate from the passband to the stopband. In order to sharpen the LPF response, some novel modifications have been introduced in this work in comparison to a traditional (basic) resonator described extensively in the literature and are depicted in Fig. 3. In fact, the modified resonator has the same fundamental behavior as the traditional basic resonator, with an improved response due to the novel modifications and optimizations that have been included in a simple symmetric structure as shown in Fig. 3. A novel equivalent LC circuit is presented and analyzed for this resonator. According to Fig. 1, in the third design step, a novel harmonic suppression is presented and analyzed. The proposed novel harmonic suppression is shown in Fig. 4 to achieve a wide stopband and suppress harmonics. Then, by adding the proposed novel harmonic suppression to the proposed novel modified resonator an LPF structure is fabricated in Fig. 5. In the final step of Fig. 1, the proposed LPF structure is integrated in both branches of conventional power divider to pass DC frequency and fundamental harmonic and omit other harmonics (2nd to 7th harmonics).

In the first design step, a compact lowpass resonator (LPR) based on the third-order LPF circuit is designed. This LPR is then used as part of a high-performance filter that is integrated into the WPD. The dimensions of the LPR are calculated by normalization coefficients of the third-order LPF circuit with $g_{L1} = 1.299$, $g_{L2} = 0.0250$, $g_{L3} = 2.142$ and $g_{C2} = 1.344$[39]. The values of the capacitors and inductors of the third-order circuit can be obtained using Eqs. (1a) and (1b). Moreover, the physical lengths of the low- and high-impedance lines are calculated using Eqs. (1c) and (1d)[39].

$$L_i = \frac{1}{2\pi f_c} Z_0 g_{Li} \tag{1a}$$

$$C_i = \frac{1}{2\pi f_c} \frac{1}{Z_0} g_{Ci} \tag{1b}$$

$$l_{Li} = \frac{\lambda_{gLi}}{2\pi} Sin^{-1}\left(\frac{2\pi f_C L_i}{Z_{0L}}\right) \tag{1c}$$

$$l_{Ci} = \frac{\lambda_{gCi}}{2\pi} Sin^{-1}\left(2\pi f_C C_i Z_{0C}\right) \tag{1d}$$

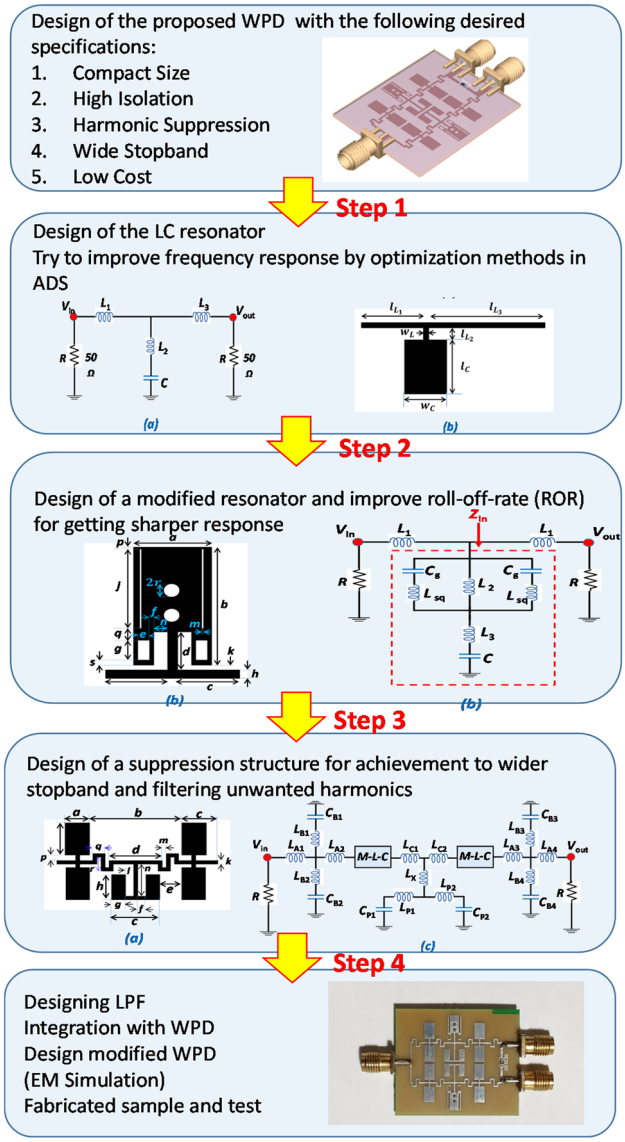

Figure 1. The design procedure of the proposed WPD.

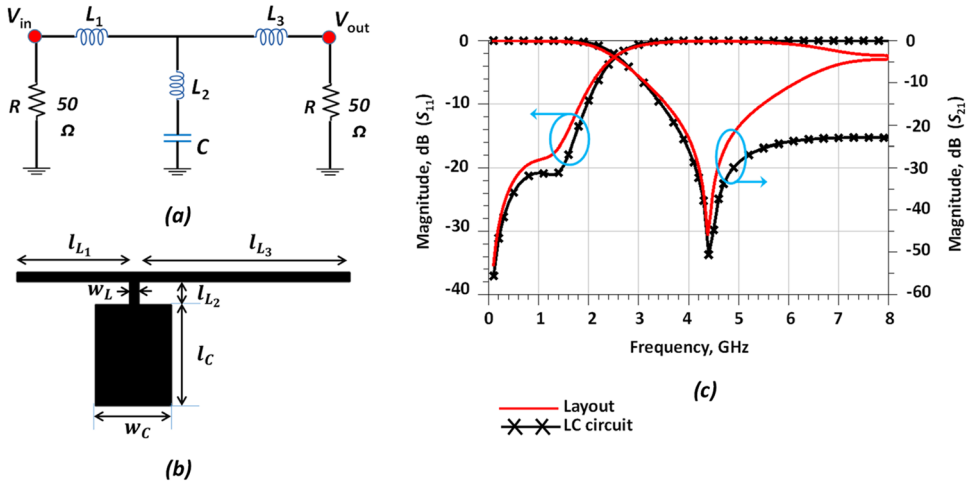

Figure 2. Proposed basic resonator. (**a**) Third-order circuit. (**b**) Layout. (**c**) Simulation results.

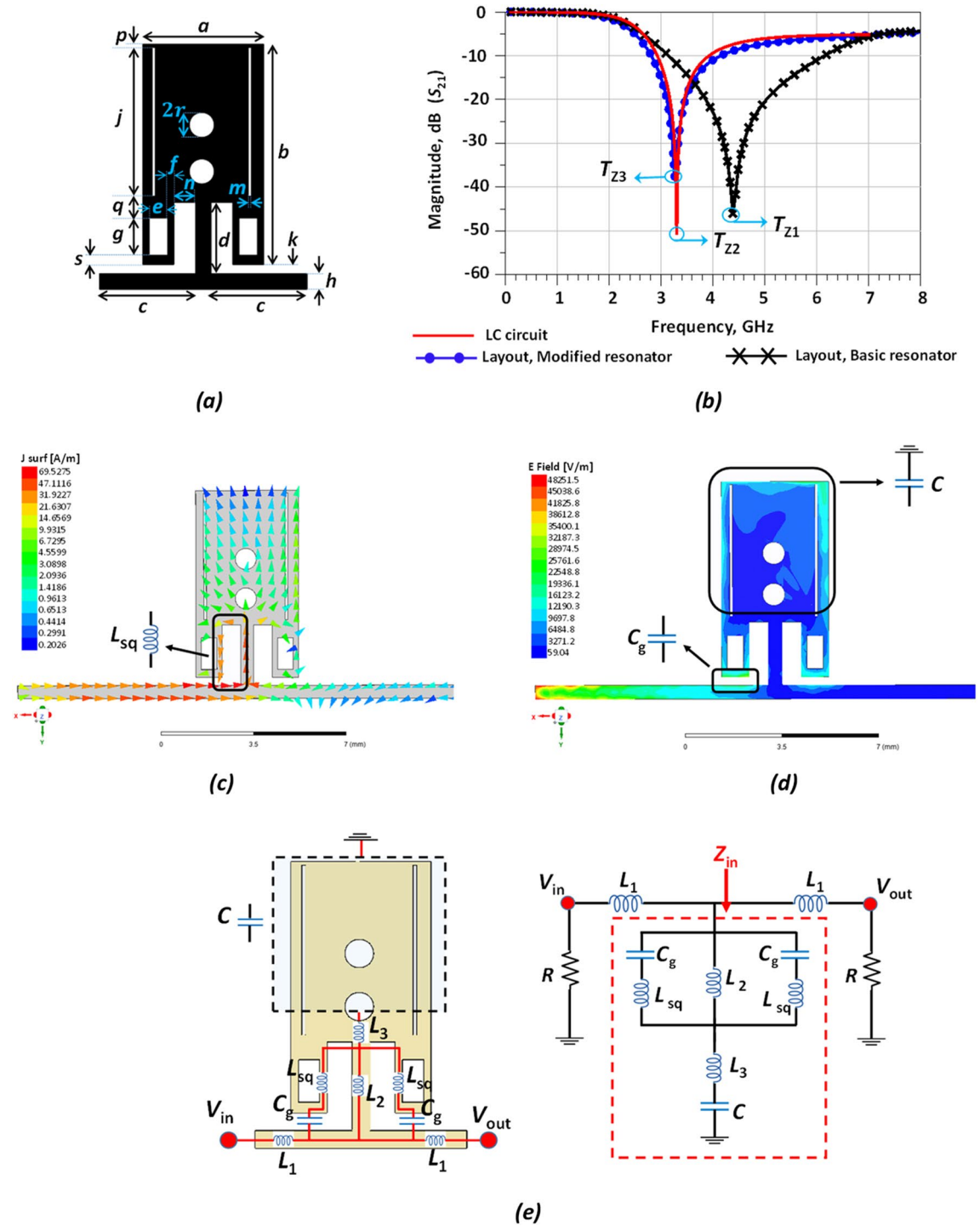

Figure 3. Proposed modified resonator. (**a**) Layout. (**b**) Simulated results. (**c**) Full wave surface current at Tz. (**d**) Electrical field strength at Tz and (**e**). LC equivalent circuit.

In the above equations, Z_0 is the characteristic impedance of the transmission line (50 Ω). The circuit configuration and PCB layout of the LPR and third-order circuit are depicted in Fig. 2. The values of the LC third-order circuit are $L_1 = 3.864$ nH, $L_3 = 2.65$ nH, $C = 1.71$ pF, and $L_2 = 0.754$ nH. The parameters λ_{gL} and λ_{gC} are the corresponding guided wavelengths, and Z_{Li} and Z_{Ci} are the impedances of transmission lines with high and low impedance, respectively. Dimensions of the LPR are specified as $W_L = 0.5$, $l_{L1} = 6.067$, $l_{L3} = 11.351$, $l_{L2} = 1.035$, $W_C = 4$ and $l_C = 4.652$ (all dimensions in mm). In order to achieve an improved filtering response (sharper ROR), the LPR needs to be optimised. This can be accomplished using built-in optimisation methods in ADS, or alternatively, implementing custom-made optimisation algorithms. Here, the ADS optimisation option was employed, and LPR dimensions were updated as follows: $W_L = 0.5$, $l_{L1} = 5.8$, $l_{L3} = 11.1$ and $l_{L2} = 1.2$; for capacitors: $W_C = 4$ and $l_C = 5.3$ have been obtained (all dimensions in mm).

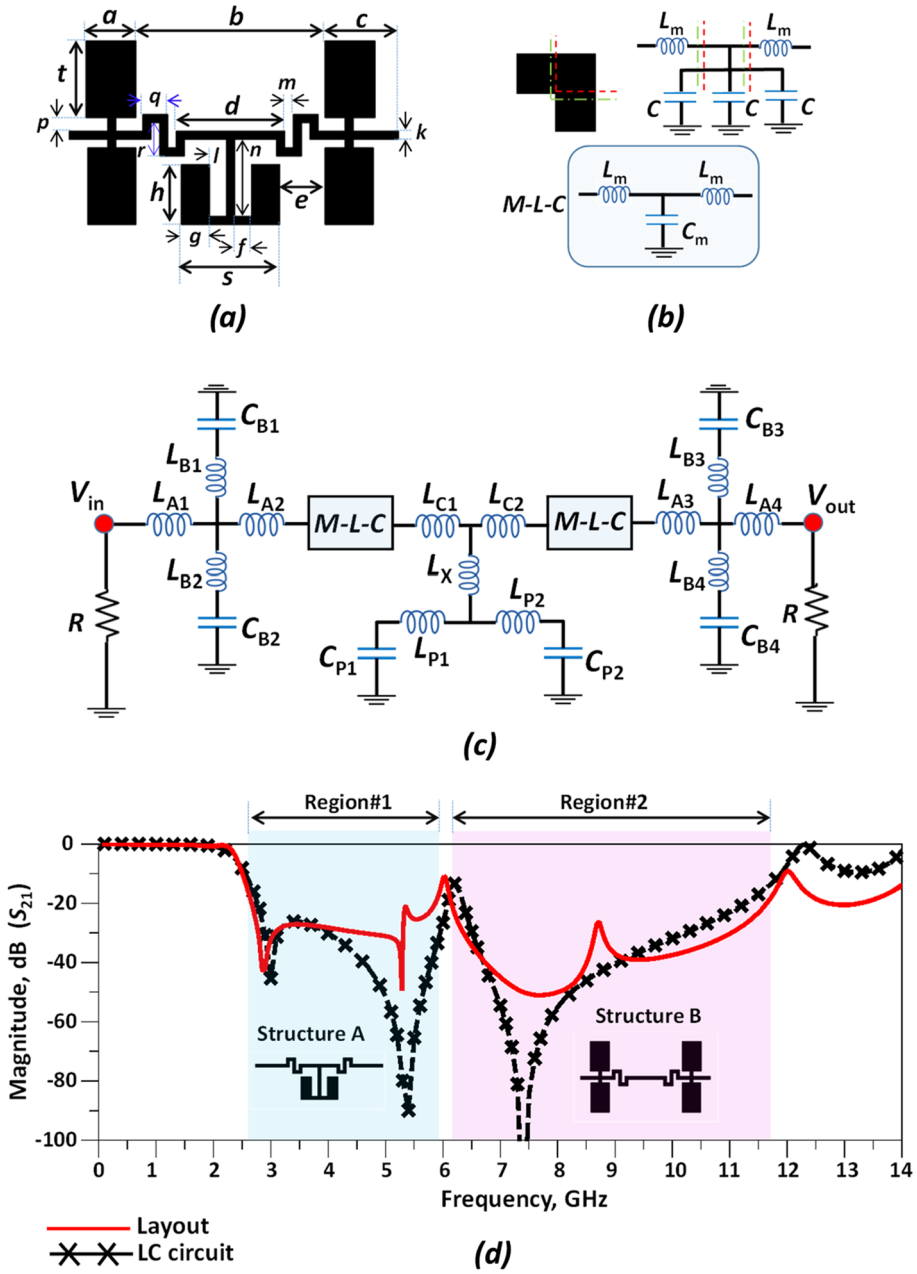

Figure 4. The suppression cell structure. (**a**) Layout. (**b**) Bending line. (**c**) Equivalent LC-circuit and (**d**) simulation results. (The optimized values of the LC-circuit are obtained as: $L_{A1,2,3,4}=0.55$ nH, $L_{C1,2}=1.2$ nH, $L_{P1,2}=1.2$ nH, $L_{B1,3}=0.84$ nH, $L_{B2,4}=1.6$ nH, $L_{m1,2,3,4}=1.1$ nH, $L_X=0.9$ nH, $C_{P1,2}=0.95$ pF, $C_{m1,2}=0.12$ pF and $C_{B1,2,3,4}=0.55$ pF).

According to Fig. 1, the first objective is to design a LPF structure (by using a modified resonator and harmonic suppression cells), and the primary design constraint is the integration of a LPF into the WPD branches to eliminate harmonics. According to Fig. 2c, a good agreement is observed between the simulation results of the layout and the LC third-order circuit. The ABCD parameters of the proposed resonator (third-order LPF circuit) are obtained as:

$$A = \frac{1-\omega^2 C(L_1+L_2)}{1-\omega^2 CL_2} \tag{1e}$$

$$B = \frac{\left[\begin{array}{c} j\omega^3 CL_2L_3 - j\omega(L_3+L_1)+ \\ j\omega^3 CL_1(L_2+L_3) \end{array}\right]}{1-\omega^2 CL_2} \tag{1f}$$

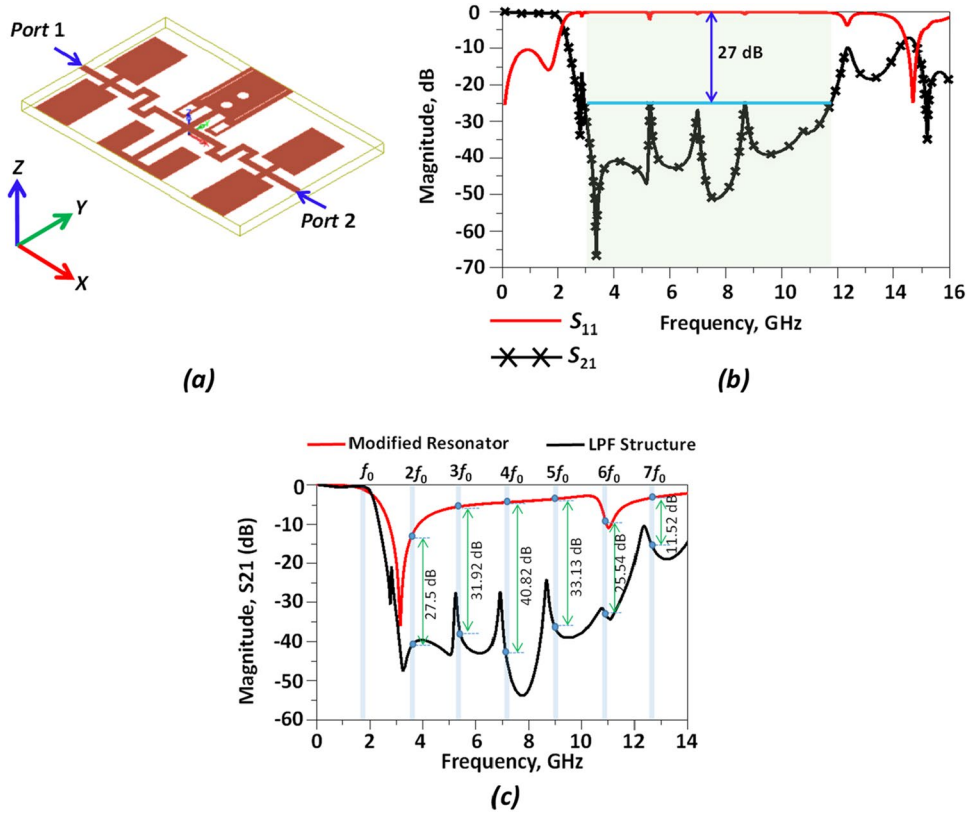

Figure 5. Proposed LPF structure. (**a**) 3D PCB Layout. (**b**) Simulated results. (**c**) Simulated results for the proposed LPF structure and modified resonator. The f_0 (1.8 GHz) is the operating frequency for the proposed WPD.

$$C = \frac{j\omega C}{1 - \omega^2 C L_2} \tag{1g}$$

$$D = \frac{1 - \omega^2 C(L_3 + L_2)}{1 - \omega^2 C L_2} \tag{1h}$$

The relationship between Insertion Loss (IL) (S_{21} parameter) the ABCD parameters referred to in Eq. (1e) to (1h) can be expressed as:

$$S_{21} = \frac{2Z_0(1 - \omega^2 C L_2)}{Z_0 K_1 + K_2 + K_3} \tag{2a}$$

$$K_1 = \left[2 - \omega^2 C(L_1 + L_3 + 2L_2)\right] \tag{2b}$$

$$K_2 = j\omega^3 C(L_2 L_3 + L_1 L_2 + L_1 L_3) \tag{2c}$$

$$K_3 = j\omega(C - L_3 - L_1) \tag{2d}$$

According to Eq. (2a), the location of the transmission zero (Tz) can be controlled by parameters C and L_2.

$$T_z \to 2Z_0\left(1 - \omega^2 C L_2\right) = 0 \tag{3}$$

$$T_Z = \frac{1}{2\pi\sqrt{L_2 C}} = \frac{1}{2\pi\sqrt{0.754 * 10^{-9} * 1.71 * 10^{-12}}}$$

$$T_Z = 4.486\text{GHz} \tag{4}$$

The transition function for the third-order circuit is defined by Eq. (5).

$$\frac{v_{out}}{v_{in}} = \frac{R\left(1 + CL_2S^2\right)}{\begin{bmatrix} R + L_1S + L_3S + CL_1RS^2 \\ +CL_2RS^2 + CL_1L_2S^3 + \\ CL_1L_3S^3 + CL_3L_2S^3 \end{bmatrix}} \tag{5}$$

According to Eq. (5), the location of the transmission zero or Tz can be controlled by parameters C and L_2.

$$T_z \to R\left(1 + S^2CL_2\right) = 0 \tag{6}$$

$$T_Z = \frac{1}{2\pi\sqrt{L_2C}} = \frac{1}{2\pi\sqrt{0.754 \times 10^{-9} \times 1.71 \times 10^{-12}}}$$

$$T_Z = 4.486\text{GHz} \tag{7}$$

According to the above equations, there is a good agreement between the Tz results for the third-order circuit. The comparison between the calculated and simulated results for Tz is illustrated in Table 1.

The sharp response (response with fast ROR) is one of the important parameters of the LPF structures that can be calculated by the following equation.

$$ROR = \frac{\alpha_{max} - \alpha_{min}}{f_s - f_c}\left(\frac{\text{dB}}{\text{GHz}}\right) \tag{8}$$

In (8), α_{max} is usually − 40 dB (or − 20 dB) and α_{min} is − 3 dB; f_s is the frequency of − 40 dB point, and f_c is the cut-off frequency. In order to sharpen the LPR response, some novel modifications are introduced to the basic resonator and are depicted in Fig. 3. The novel equivalent LC circuit of the modified LPR is also depicted to provide a better insight into the filtering mechanism.

According to the Fig. 3b, the ROR parameter for the basic resonator and modified resonator are obtained as 18.28 dB/GHz and 61.15 dB/GHz, respectively. The location of Tz for the basic and modified resonators are in the vicinity of 4.48 GHz (with 44.86 dB) and 3.27 GHz (with 38.48 dB), respectively. The dimensions of the modified resonator have been optimized in ADS. The optimized length and width values for the modified resonator are: $a = 3.9$, $b = 7.1$, $c = 3.1$, $d = 2.3$, $e = 0.6$, $f = 0.2$, $g = 1.2$, $h = 0.5$, $j = 4.8$, $k = 0.3$, $m = 0.1$, $n = 0.7$, $p = 0.1$, $q = 0.7$, $r = 0.4$ and $s = 0.3$ (all in mm). The input impedance (Z_{in}) for the main branch of the equivalent LC circuit (depicted in Fig. 3e) is calculated in Eq. (9).

$$Z_{in} = \frac{\alpha S^4 + \beta S^2 + 1}{SC\left[S^2\left(C_gL_{sq} + L_2C_g\right) + 1\right]} \tag{9}$$

$$\alpha = L_{sq}C_gL_2C + L_3C_gL_{sq}C + 2L_3C_gL_2C \tag{10}$$

$$\beta = L_2C + L_3C + L_{sq}C_g + 2L_2C_g \tag{11}$$

According to Eq. (12), the location of T_Z can be obtained by the following equations:

$$T_Z = \pm\sqrt{\frac{1}{4\pi^2}} \times \sqrt{\frac{\beta \pm \sqrt{k}}{2CC_g(2L_2L_3 + L_2L_{sq} + L_3L_{sq})}} \tag{12}$$

$$K = \left[C^2L_2^2 + 2C^2L_2L_3 + C^2L_3^2 + 4CC_gL_2^2 - 4CC_gL_2L_3 - 2CC_gL_2L_{sq} - 2CC_gL_3L_{sq} + 4C_g^2L_2^2 + 4C_g^2L_2L_{sq} + C_g^2L_{sq}^2\right] \tag{13}$$

The inductance and capacitance values for the equivalent LC circuit for the modified LPR were optimized to $L_1 = 1.2$ nH, $L_2 = 0.6$ nH, $L_3 = 1.5$ nH, $C_g = 0.2$ pF, $L_{sq} = 0.4$ nH and $C = 1.2$ pF. According to Table 2, there is a

Tz (GHz)	Equation (4)	Equation (7)	Simulation LC-circuit and layout
Tz(GHz)	4.486	4.486	4.462

Table 1. Comparison between calculated and simulated results for Tz for the basic resonator.

Tz	Equation (12)	Layout	Simulation LC-circuit
	3.125 GHz	3.271 GHz	3.127 GHz

Table 2. Comparison between calculated and simulated results for the Tz of the modified resonator.

small difference in the results between the *Tz* and modified LPR. The comparison between the calculated and simulated results for *Tz* is depicted in Table 2.

A more accurate equivalent circuit of the proposed resonator is extracted based on the EM simulations. The surface current and electrical field distribution are shown in Fig. 3c,d to clarify the proposed LC circuit in Fig. 3e. According to the above explanation, LC circuit and layout for the basic resonator are conventional, but they have been used for creating a novel modified resonator. Moreover, the proposed modified resonator and presented LC circuit based on surface current and electrical field in a full wave simulation are more accurate, symmetric and novel.

To achieve a wide stopband and improve the frequency response in the rejection band, a suppression structure has been added to the modified LPR. The suppression structure is shown in Fig. 4. The proposed suppression cell consists of two structures (structures A and B) regarding to the Fig. 4d to suppress S_{21} in the rejection band in Region#1 and region#2, respectively and creating a wide stopband. The suppressor cell causes pulldown of the IL parameter in the stopband in the range of 2.65–5.88 GHz (Region#1 in Fig. 4) and 6.16–11.68 GHz (Region#2 in Fig. 4) with more than 20 dB attenuation level. The length and width values of the suppressor cell are: $a=3$, $b=11.3$, $c=4.4$, $d=6.5$, $e=2.7$, $f=1$, $g=1.7$, $h=3.6$, $k=0.5$, $l=1$, $m=0.5$, $n=4.6$, $p=0.8$, $q=1.5$, $r=2$, $s=5.9$ and $t=4.6$ (all in mm). The layout, equivalent LC circuit and simulation results for the proposed suppression cell structure are illustrated in Fig. 4. According to the Fig. 4d, a good agreement is observed between the layout and equivalent LC circuit results. In order to create a wider stopband, more suppression structures are required which results in a sophisticated LC circuit with a complex structure, so there is a tradeoff between the number of suppression structures and creating a wider stopband. The proposed LPF structure is designed and analyzed in the remainder of this section.

The introduction of the suppressor cell to the modified LPR yields a LPF with a sharp response and large stopband as depicted in Fig. 5. Table 3 illustrates the comparison of the proposed LPF with some of the recent filters in the literature from the same class. The − 3 dB cut-off frequency for the proposed LPF is 2.16 GHz. The frequency response (ROR parameter) is sharp and equal to 53 dB/GHz. The transition band is narrow and covers a frequency band from 2.16 to 2.76. The IL and RL in the passband and stopband are better than 0.4, 10.6, 20 and 0.3 dB, respectively. The suppression level across 90% of the stopband is better than 27 dB leading to SF parameter being 2.7. The stop bandwidth is also desirably large and covers a 9.1 GHz range (2.88–11.98 GHz), with an RSB of 1.23 having been obtained.

After designing the modified resonator, a suppression cell structure is presented in Fig. 4 which is envisaged to create a wider stopband for the proposed LPF structure. In fact, the final LPF structure (in Fig. 5a) consists of the modified resonator and the suppression cell structure. According to the Fig. 5c, there is a significant reduction in the harmonic levels (for 2nd to 7th harmonics). According to this figure, all the unwanted harmonics (2nd to 7th) have been located in the stopband region of the proposed LPF. The operation for the proposed LPF structure developed to suppress harmonics has been illustrated in Fig. 5c. The proposed LPF structure will be integrated in both branches of a conventional WPD to create a wide stopband and suppress harmonics in the next section.

Power divider structure design

A conventional microstrip WPD is designed by implementing two quarter wave-length microstrip lines ($\lambda/4$ transmission lines) with a characteristic impedance of 70.7 Ω ($\boldsymbol{Z}_0\sqrt{2}\boldsymbol{\Omega}$ and a 100 Ω terminating resistor. A schematic for the block diagram and simulation results of the proposed conventional WPD are shown in Fig. 6. According to the simulation results, the input return loss (S_{11}), insertion loss (S_{21}) and isolation (S_{32}) at 1.8 GHz are better than 46.85 dB, 3.17 dB and 44.72 dB, respectively. The proposed LPF structure is integrated into both branches of conventional power divider as a means for improving harmonic suppression and achieving a sharper response with a wider stopband. The proposed modified WPD is depicted in Fig. 7.

The even and odd mode circuits which form the critical building blocks for the modified WPD are illustrated in Fig. 8. The expressions for calculating the even and odd mode parameters are described in detail in Appendix (Additional/Supplementary Information)

Discussion of results and contributions

The proposed power divider has been implemented on a low-cost FR4 substrate with a dielectric constant of 4.4, a thickness of 0.8 mm (~ 31 mil) and a loss tangent 0.022. The fabricated prototype WPD and measured results are depicted in Fig. 9.

References	f_c (GHz)	ROR (dB/GHz)	RSB	SF	Size (λg^2)	IL (dB)
[7]	1.9	37	1.45	1.8	–	0.3
[9]	1.9	85	1.43	2.5	0.31 × 0.21	0.5
[10]	1	78	–	2	0.16 × 0.1	0.3
[11]	2.68	42.5	1.51	2	–	0.12
[14]	0.9	80			0.17 × 0.10	0.5
[15]	2	123	1.65	2	–	0.3
This work	2.16	53	1.23	2.7	0.24 × 0.16	0.4

Table 3. Comparison between simulated results and other studies for LPF.

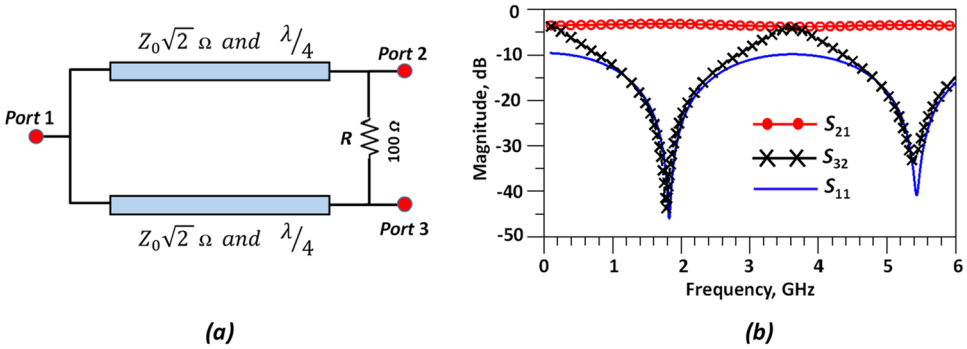

Figure 6. Conventional WPD. (**a**) Schematic and (**b**) simulation results.

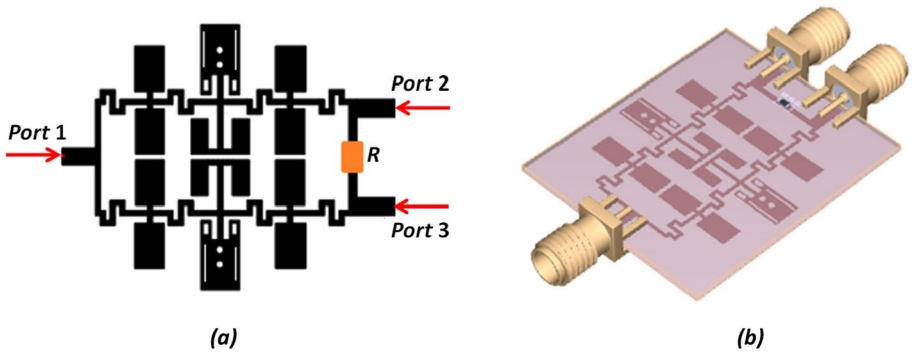

Figure 7. Modified WPD. (**a**) PCB Layout and (**b**) 3D-Schematic.

The simulated and measured results for the modified WPD are shown in Fig. 10 with the frequency varying between 0.1 and 6 GHz. A R&S ZVL13 Vector Network Analyzer was used to measure the *S*-parameters response with a frequency range of 0.1–13.6 GHz during measurements. According to the results, there is a good agreement between the simulated and measured results.

The isolation between output ports ($|S_{32}|$), input return loss ($|S_{11}|$) and insertion loss ($|S_{21}|$) are better than 31.2 dB, 34.2 dB and 3.52 dB, respectively, at 1.8 GHz. The simulated results over the frequency range of 0.1–16 GHz and the measured results in the range of 0.1–13.6 GHz are presented in Fig. 11.

As observed, there is good agreement between the simulated and measured results. Figure 12 shows the harmonic suppression level and stopband bandwidth of the proposed modified and conventional WPDs. According to the results, the proposed WPD has a wide stopband from 2.53 to 12.21 GHz and 2.54 to 13.48 GHz with 20 dB attenuation levels for both the simulated and measured results, respectively. According to Fig. 12, the proposed modified WPD can provide additional attenuation of unwanted signals and harmonics in the stopband region. The second to seventh harmonics at frequencies $2f_0$ to $7f_0$ ($f_0 = 1.8$ GHz) are shown to be suppressed with better than 51.2, 40.3, 51.36, 37.5, 42.9 and 28.2 (all in dB) attenuation levels. By comparison with the literature for modified and conventional WPDs, desirable suppression levels in the rejection band are demonstrated for the proposed WPD structure and unwanted signals and harmonics have been greatly attenuated in this region.

Figure 13 plots the simulated values for magnitude and phase imbalance as well as group delay. It can be seen from the results that the modified WPD exhibits a magnitude imbalance of 0.002, a phase imbalance of – 0.152 degree and a group delay of 0.73 ns. These results compare very favorably with the literature and demonstrate the symmetrical nature of the proposed structure.

Table 4 depicts a comparison between the obtained results and other works described in the literature. As can be seen in Table 4, the proposed modified WPD performs well in comparison to other reported works. The output isolation is seen to perform well and shows improved measurements when compared to the isolation results reported in[18–26,28–32,40–42]. The input and output return loss have been obtained and also show an improvement over the results described in such works as[18–43]. In terms of the stopband, the WPD also has a large stopband, extending from 2.54 to 13.48 GHz. This is greater than the stopbands reported in[18–23,26–43]. The presented WPD omits the second to seventh unwanted harmonics with higher suppression levels in comparison with other works[18–21,23,24,26–43]. As can be seen from the comparison table (Table 4), the proposed modified WPD shows superior performance compared to the other works where various WPD technologies have been reported[44–46]. In relation to the novelty of the proposed structure, an LPF with LC equivalent circuits was inserted in both branches of the WPD to realize a novel power divider (PD). The major size of the proposed WPD belongs to the LPF and its dimension is inversely proportional to the frequency of operation and order of the filter. Indeed, a WDP with higher ROR requires higher order filter which consequently increases the size of the LPF. Therefore,

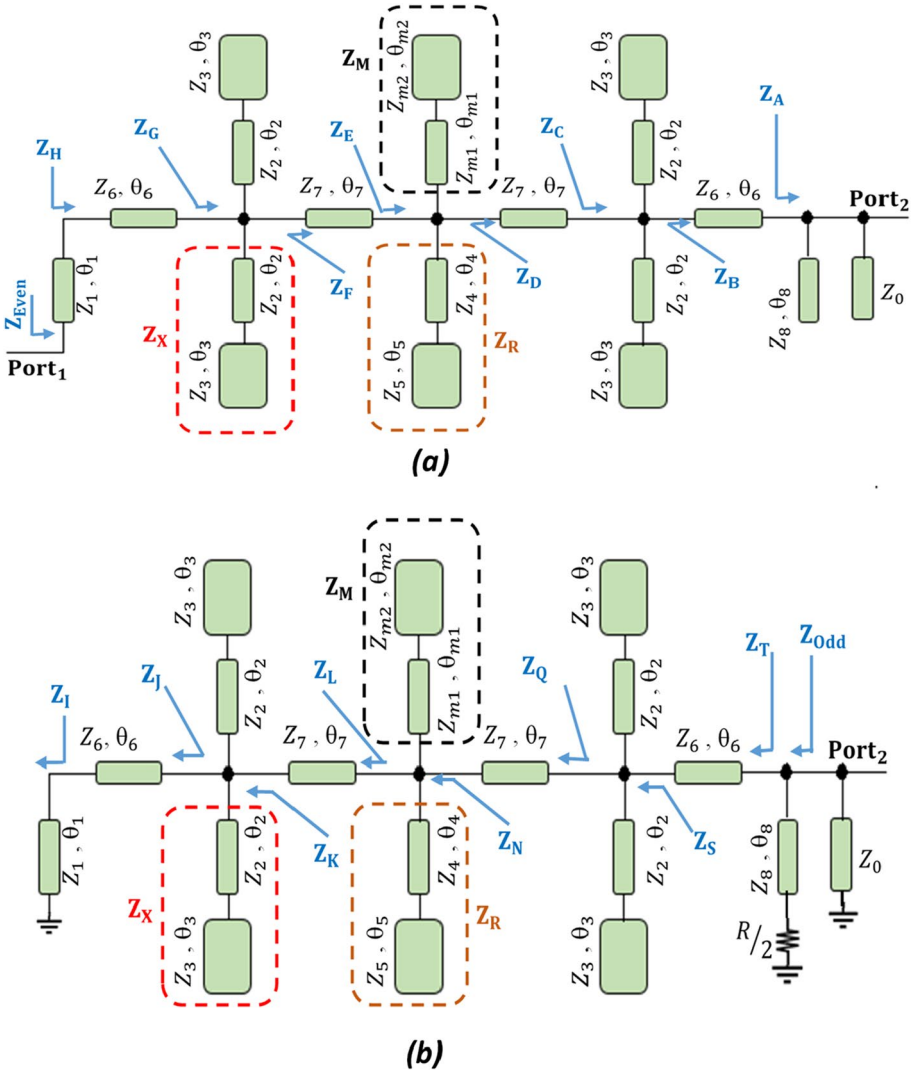

Figure 8. Equivalent circuit of the modified WPD. (**a**) Even mode and (**b**) odd mode.

there is a trade-off between the size of the structure and the performance of the WPD, particularly with respect to ROR, SF and wide stopband results.

There are several positive aspects regarding novelty, contribution and design methodology that have been described in detail throughout this paper. In this paper, an effort to establish a novel modified WPD with good performance characteristics using a new, simple and low cost structure for operation at 1.8 GHz in GSM and LTE communication applications has been accomplished and described. To summarise the contributions and strengths of this research work, the benefits of the proposed modified WPD are summarized as follows.

- LPF structure: in this work, a third-order LPF has been designed based on the techniques and equations described in[39]. In the proposed work, a sharper frequency response is achieved using a novel modified resonator with the LC equivalent circuit for all structures and *Tz* calculation described in detail.
- Modified WPD structure: although conventional WPDs can provide acceptable results around the center frequency, the out-of-band response is quite poor. In contrast, the WPD presented in this work also demonstrates good performance for the out-of-band performance: in other words, the WPD exhibits a high isolation level, high output and input RL, low IL in the passband region with high suppression level in the stopband. Moreover, the presented WPD provides a large attenuation of the second to seventh harmonics in the range of 2.54–13.48 GHz.
- Integration: the design and fabrication of multiport systems with improved performance characteristics are still a challenge for microwave researchers. In this paper, the presented LPF structure has been replaced in both branches of a conventional WPD as a means of improving harmonic suppression.
- Affordable: the size and cost of implementation are key factors to consider, so in this work, a key goal was to reduce circuit size to achieve a simple structure. A commercial high-frequency FR4 substrate with low cost and high accessibility has therefore been used in this work to ensure low cost of manufacture.

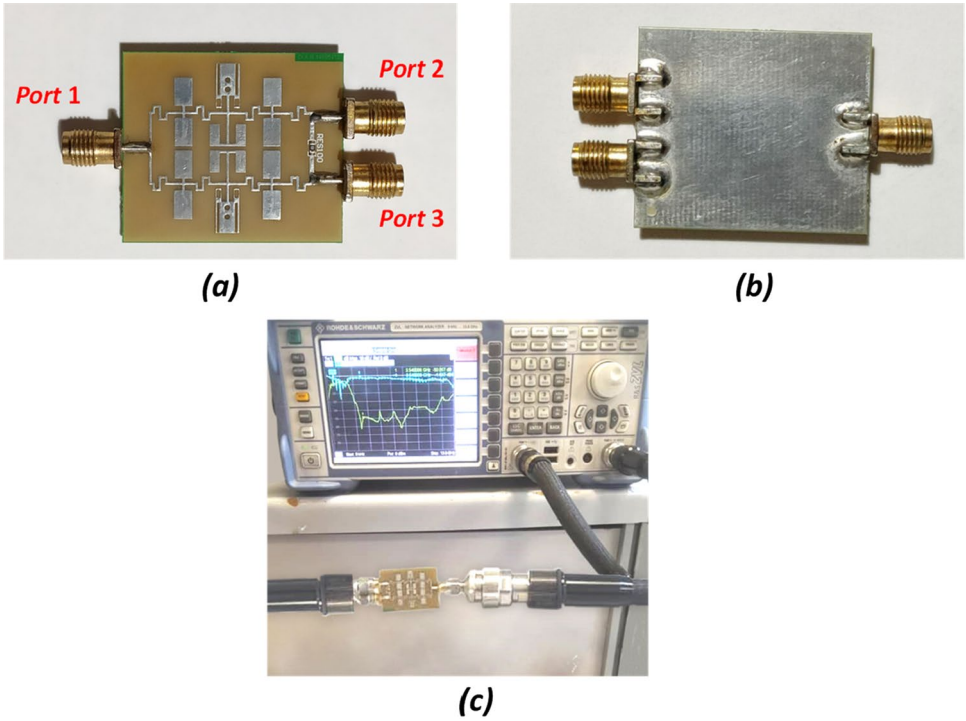

Figure 9. Fabricated sample of modified WPD. (**a**) Top, (**b**) bottom, (**c**) test setup.

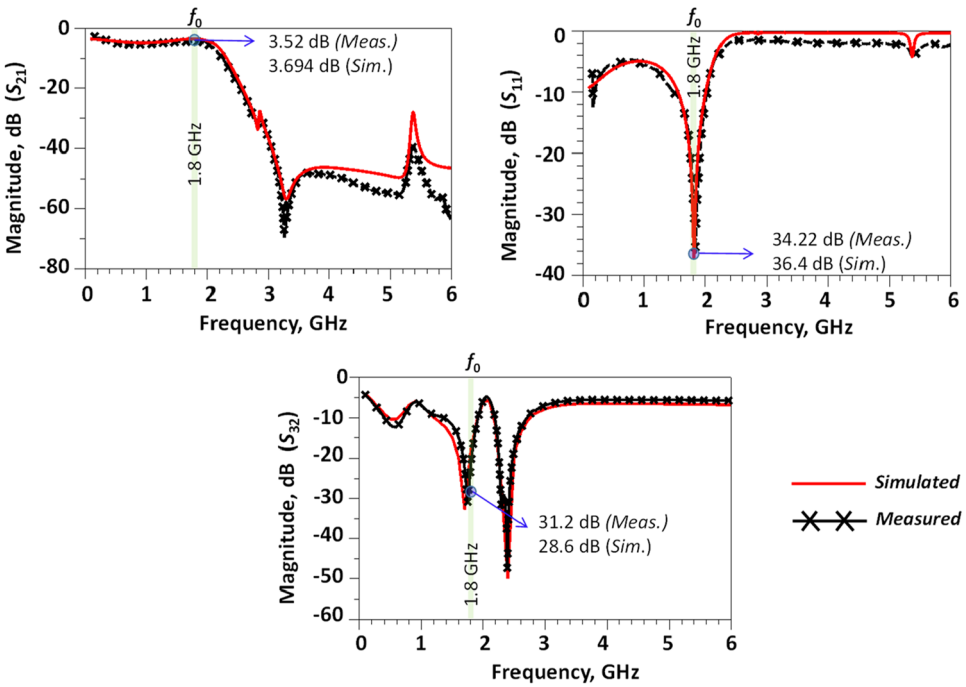

Figure 10. Simulated and measured results (0.1–6 GHz) for the proposed modified WPD.

- Excellent results: according to Table 4, the WPD performance compares very well with, and improves on, the existing state-of-the-art. For instance, harmonic suppression for the second to seventh harmonics have been achieved with greater than 51.2, 40.3, 51.36, 37.5, 42.9 and 28.2 (all in dB) attenuation levels, respectively across a frequency range from 2.54 to 13.48 GHz.
- Applications: among power dividers, WPDs are widely used due to their simple construction, narrow bandwidth, and reliable performance. WPDs can be used in test systems to measure two different characteristics of a signal, such as frequency and power, for broadband-independent signal sampling. GSM modems have a

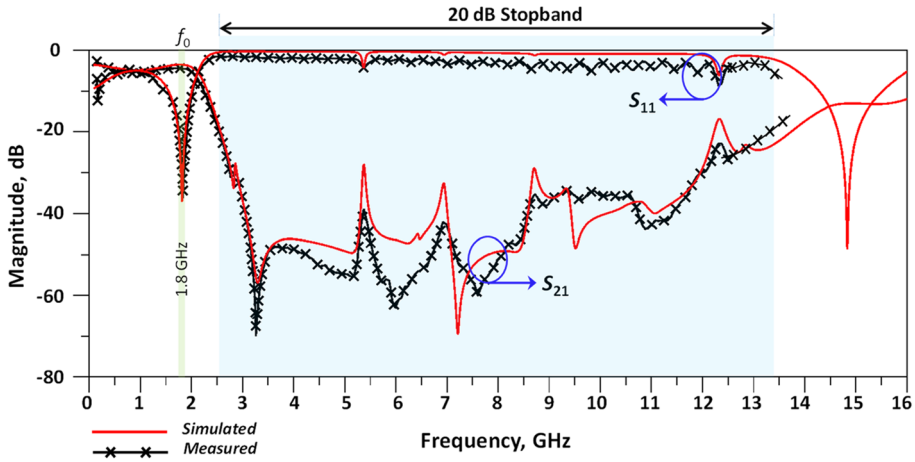

Figure 11. Simulated (0.1–16 GHz) and measured results (0.1–13.6 GHz) for the proposed modified WPD.

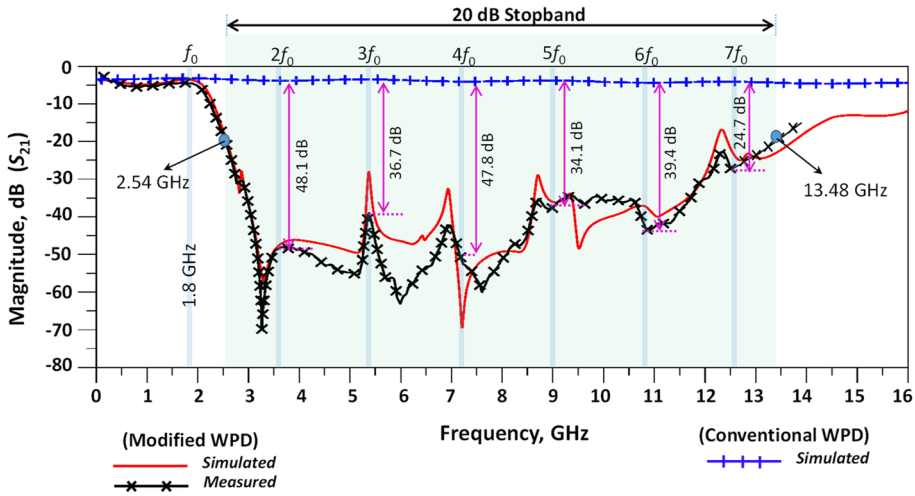

Figure 12. Harmonic suppression, simulation (0.1–16 GHz) and measurement (0.1–13.6 GHz) results of proposed conventional and modified WPDs.

wide range of applications in transaction terminals, supply chain management, and security applications. One of the common frequency bands for GSM is 1800 MHz and the proposed WPD shows good performance at this frequency, in terms of having a wide stop band, high isolation, and suppression of unwanted harmonics. In modern wireless communication systems, power dividers and filters are significant components used in non-linear circuits such as detectors[6], power amplifiers[47,48], mixers[49], active circulators, and phase shifters[50]. Consequently, WPDs are designed to suppress unwanted harmonics that are generated based on non-linear electronics devices (harmonic balance theory) such as diodes and transistors. In this paper, the operating frequency is 1.8 GHz, and the proposed LPF structure can pass this frequency and suppress other harmonics. One such harmonic is the second harmonic ($2f_0 = 3.6$ GHz) that lies in close proximity to the 5G New-Radio (NR) N-77 frequency band[51], that should be suppressed for avoiding frequency interference. The presented WPD has been designed for operation at 1.8 GHz, so it can be used in next generation microwave circuits and state-of-the-art wireless communication systems for LTE and GSM services.

Conclusion

This paper has presented a novel modified WPD with high isolation and high attenuation levels in the stopband. The desirable performance of the power divider is mainly attributed to a highly tailored LPF structure that has been incorporated in the WPD, removing harmonics up to the 7th harmonic and contributing to high isolation levels. The demonstrated results show an IL better than 3.52 dB at the operating frequency with an input RL and isolation greater than 34.2 dB and 31.2 dB, respectively. There is good agreement between the simulated and measured results. The proposed WPD is therefore suitable for use in a wide range of modern wireless communication systems in GSM and LTE services.

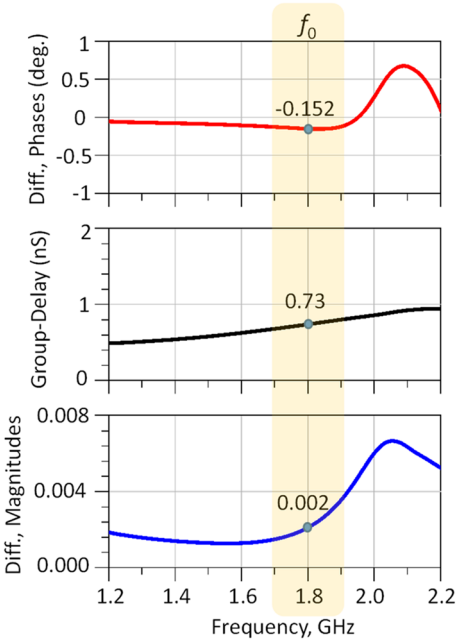

Figure 13. Group delay and magnitude and phase imbalance for the proposed WPD.

References	f_0 (GHz)	Isolation, S_{32} (dB)	S_{11} (dB)	S_{21} (dB)	S_{22} (dB)	Harmonics suppression	Size (λg^2)	Stopband (GHz)
[18]	1.8	15.2	16.5	4	14.3	–	0.036 × 0.02	–
[21]	2.05	10.2	10.1	3	~15	2nd	–	2.98 to 4.93
[22]	0.7	>28	>20	3.2	>25	2nd–15th	0.11 × 0.044	2.9 to 10.5
[23]	1	20	20	3.25	20	2nd–4th	–	1.94 to 4.26
[24]	2.45	11.8	>25	3.4	–	2nd–7th	0.19 × 0.25	4.8 to 19.92
[25]	1.8	20.1	21.2	3.1	–	2nd-11th	0.31 × 0.16	4.4 to 19.9
[26]	1.8	20	20	3.6	20	2nd-3rd	–	–
[27]	1.8	34.6	20.1	3.1	20	2nd–6th	0.14 × 0.16	3.41 to 10.9
[28]	1.5	–	40	3.2	–	2nd-3rd	–	–
[29]	2.65	22	27	3.4	–	3rd–5th	–	–
[30]	1	20	18	0.52	22	2nd–4th	–	1.8 to 4
[32]	1.5	23.8	19.97	3.22	–	2nd–5th	–	~3.3 to 7.9
[43]	1.8	35	34	3.2	–	2nd–7th	0.28 × 0.14	~4 to 13.2
[40]	1.74	23	34	3.3	23	2nd–5th	0.11 × 0.13	~3.1 to 9.1
[41]	4.11	17	22	3.8	–	–	0.29 × 0.45	–
[42]	1	13.5	30	>3.4	–	2nd–5th	–	–
[44]	0.9	23	>20	4.75	>20	–	0.10 × 0.2	–
This work	1.8	31.2	34.2	3.52	26.2	2nd–7th	0.42 × 0.33	2.54 to 13.48

Table 4. Comparison of the proposed modified Wilkinson power divider with related works in the literature.

Data availability

The datasets used and/or analyzed during the current study are available from the corresponding author on reasonable request.

Received: 14 September 2022; Accepted: 6 March 2023
Published online: 14 March 2023

References

1. Bahrami, S., Moloudian, G., Song, H.-J. & Buckley, J. L. reconfigurable UWB circularly polarized slot antenna with three modes of operation and continuous tuning range. *IEEE Trans. Antennas Propag.* **70**(9), 8542–8547 (2022).

2. Bahrami, S., Moloudian, G., Miri-Rostami, S. R. & Bjorninen, T. Compact microstrip antennas with enhanced bandwidth for the implanted and external subsystems of a wireless retinal prosthesis. *IEEE Trans. Antennas Propag.* **69**(5), 2969–2974 (2021).
3. Yeo, J. & Lee, J.-I. Design of a high-sensitivity microstrip patch sensor antenna loaded with a defected ground structure based on a complementary split ring resonator. *Sensors* **20**, 7064 (2020).
4. Zhao, L. *et al.* A novel broadband band-pass filter based on spoof surface plasmon polaritons. *Nat. Sci. Rep.* **6**, 36069. https://doi.org/10.1038/srep36069 (2016).
5. Al-Yasir, Y. I. A., Ojaroudi Parchin, N., Abdulkhaleq, A. M., Bakr, M. S. & Abd-Alhameed, R. A. A survey of differential-fed microstrip bandpass filters: Recent techniques and challenges. *Sensors* **20**, 2356 (2020).
6. Moloudian, G., Bahrami, S. & Hashmi, R. M. A microstrip lowpass filter with wide tuning range and sharp roll-off response. *IEEE Trans. Circ. Syst. II Express Briefs* **67**(12), 2953–2957 (2020).
7. Chen, C. J. Design of artificial transmission line and low-pass filter based on aperiodic stubs on a microstrip line. *IEEE Trans. Compon. Packag. Technol.* **4**(5), 922–928 (2014).
8. Moloudian, G. & Bahrami, S. Design and fabrication of a continuous tunable microstrip lowpass filter with wide stopband and sharp response. *Int. J. RF Microw. Comput. Aided Eng.* **29**(8), e21759 (2019).
9. Cao, S., Han, Y., Chen, H. & Li, J. An ultra-wide stop-band LPF using asymmetric Pi-shaped Koch fractal DGS. *IEEE Access* **5**, 27126–27131 (2017).
10. Chen, F. C., Hu, H. T., Qiu, J. M. & Chu, Q. X. High-selectivity low-pass filters with ultrawide stopband based on defected ground structures. *IEEE Trans. Compon. Packag. Technol.* **5**(9), 1313–1319 (2015).
11. Sheikhi, A., Alipour, A. & Abdipour, A. Design of compact wide stopband microstrip low-pass filter using T-shaped resonator. *IEEE Microw. Wirel. Component Lett.* **27**(2), 111–113 (2017).
12. Moloudian, G., Dousti, M. & Ebrahimi, A. Design and fabrication of a compact microstrip low-pass filter with ultra-wide stopband and sharp roll-off-rate. *J. Electromagn. Waves Appl.* **32**(6), 713–725 (2018).
13. Salehi, A., Moloudian, G. & Setoudeh, F. Design, simulation and manufacturing microstrip low-pass filter by wide stopband and changing fast situation from passing state to stopping. *IETE J. Res.* **65**(4), 487–493 (2019).
14. Chen, F.-C., Li, R.-S. & Chu, Q.-X. Ultra-wide stopband low-pass filterusing multiple transmission zeros. *IEEE Access* **5**, 6437–6443 (2017).
15. Zhang, W. & Wang, G. Design of compact planar lowpass filters by using fragment-type structure with multi-bit scheme. *IEEE Access* **9**, 74143–74154 (2021).
16. Liu, F. X., Wang, Y., Zhang, X. Y., Quan, C. H. & Lee, J. C. A size-reduced tri-band Gysel power divider with ultra-wideband harmonics suppression performance. *IEEE Access* **6**, 34198–34205 (2018).
17. Karimi-Nobandegani, A. & Hosseini, S. E. Gysel power divider realized by ridge gap waveguide technology. *IEEE Access* **9**, 72103–72110 (2021).
18. Pakasiri, C. & Wang, S. Dual-band compact Wilkinson power divider using common inductor and complex load. *IEEE Access* **8**, 97189–97195 (2020).
19. Maktoomi, M. A. & Hashmi, M.-S. A performance enhanced port extended dual-band Wilkinson power divider. *IEEE Access* **5**, 511832–511840 (2017).
20. Lin, Y.-S. & Lan, K.-S. Spiral-coupled-line-based Wilkinson power divider. *IEEE Microw. Wirel. Compon. Lett.* **31**(3), 241–244 (2021).
21. Gao, S. S., Sun, S. & Xiao, S. A novel wideband bandpass power divider with harmonic-suppressed ring resonator. *IEEE Microwave Wirel. Compon. Lett.* **23**(3), 119–121 (2013).
22. Roshani, S. & Roshani, S. Design of a compact LPF and a miniaturized Wilkinson power divider using aperiodic stubs with harmonic suppression for wireless applications. *Springer Wirel. Netw.* **26**, 1493–1501 (2020).
23. Cheng, K. K. & Ip, W. C. A novel power divider design with enhanced spurious suppression and simple structure. *IEEE Trans. Microw. Theory Tech.* **58**(12), 3903–3908 (2010).
24. Wang, Y., Zhang, X. Y., Liu, F. X. & Lee, J. C. A compact bandpass Wilkinson power divider with ultra-wide band harmonic suppression. *IEEE Microw. Wirel. Compon. Lett.* **27**(10), 888–890 (2017).
25. Karimi-khorrami, S. & Moloudian, G. Design and fabrication of a microstrip lowpass filter with wide tuning range as harmonic suppression with application in Wilkinson power divider. *Springer Analog Integrated Circ. Signal Process.* **107**, 155–163 (2021).
26. Zhang, F. & Li, C. F. Power divider with microstrip electromagnetic bandgap element for miniaturisation and harmonic rejection. *Electron. Lett.* **44**(6), 422–424 (2008).
27. Moloudian, G., Miri-Rostami, S. R. & Bjorninen, T. Modified Wilkinsonpower divider with harmonics suppression and compact size for GSM applications. *Int. J. RF Microw. Comput. Aided Eng.* **30**(7), e22209 (2020).
28. Woo, D.-J. & Lee, T.-K. Suppression of harmonics in Wilkinson power divider using dual-band rejection by asymmetric DGS. *IEEE Trans. Microw. Theory Tech.* **53**(6), 2139–2144 (2005).
29. Wang, J., Ni, J., Guo, Y. & Fang, D. Miniaturized microstrip wilkinson power divider with harmonic suppression. *IEEE Microwave Wirel. Compon. Lett.* **19**(7), 440–442 (2009).
30. Mirzavand, R., Honari, M., Abdipour, A. & Moradi, G. Compact microstrip Wilkinson power dividers with harmonic suppression and arbitrary power division ratios. *IEEE Trans. Microw. Theory Tech.* **61**(1), 61–68 (2013).
31. Hongyu, Z. & Hayashi, H. Wilkinson power divider with broadband harmonic suppression using radial open stubs. In *IEEE 7th Global Conference on Consumer Electronics (GCCE)*, 836–837 (2018).
32. Wang, Z., Zhang, N., Wang, X., Ma, Z. & Chen, C.-P. Miniaturized horst-type Wilkinson power divider with harmonic suppression. In *IEEE Asia-Pacific Microwave Conference (APMC)*, 881–883 (2020).
33. Yang, Y. *et al.* Development of a wideband 220-GHz sub harmonic mixer based on GaAs monolithic integration technology. *IEEE Access* **8**, 31214–31226 (2020).
34. Rayatzadeh, S. & Moloudian, G. Design and fabrication of a miniaturized lowpass-bandpass diplexer with wide tuning range and high isolation. *J. Electromagn. Waves Appl.* **33**(14), 1874–1889 (2019).
35. Moloudian, G., Dousti, M. & Ebrahimi, A. Design and fabrication of a tunable microstrip lowpass-bandpass diplexer for telecommunication applications. *Microw. Opt. Technol. Lett.* **60**(3), 754–759 (2018).
36. Chen, C.-F., Zhou, K.-W., Chen, R.-Y., Wang, Z.-C. & He, Y.-H. Design of a microstrip diplexer-integrated filtering power divider. *IEEE Access* **7**, 106514–106520 (2019).
37. Deng, P., Liu, R., Lin, W. & Lo, W. Design of a microstrip low-pass-bandpass diplexer using direct-feed coupled-resonator filter. *IEEE Microw. Wirel. Compon. Lett.* **27**(3), 254–256 (2017).
38. Moloudian, G. & Dousti, M. Design and fabrication of a compact microstrip lowpass-bandpass diplexer with high isolation for telecommunication applications. *Int. J. RF Microw. Comput. Aided Eng.* **28**(5), e21248 (2018).
39. Hong, J.-S. & Lancaster, M. J. *Microstrip Filters for RF/Microwave Applications* (Wiley, 2004).
40. Jamshidi, M. *et al.* A neuro-based approach to designing a Wilkinson power divider. *Int. J. RF Microw. Comput. Aided Eng.* **30**(3), e22091 (2019).
41. Sajadi, A., Sheikhi, A. & Abdipour, A. Analysis, simulation, and implementation of dual-band filtering power divider based on terminated coupled lines. *IEEE Trans. Circ. Syst. II Express Briefs* **67**(11), 2487–2491 (2020).
42. Coromina, J., Vélez, P., Bonache, J. & Martín, F. Branch line couplers with small size and harmonic suppression based on non-periodic step impedance shunt stub (SISS) loaded lines. *IEEE Access* **8**, 67310–67320 (2020).

43. Lalbakhsh, A. *et al.* Design of a compact planar transmission line for miniaturized rat-race coupler with harmonics suppression. *IEEE Access* **9**, 129207–129217 (2021).
44. Chau, W.-M., Hsu, K.-W. & Tu, W.-H. Filter-based Wilkinson power divider. *IEEE Microw. Wirel. Compon. Lett.* **24**(4), 239–241 (2014).
45. Moloudian, G., Lalbakhsh, G. & Bahrami, S. A harmonic-free Wilkinson power divider using lowpass resonators. In *IEEE, Proceedings of the European Conference on Antennas and Propagation (EUCAP)* (2022).
46. Jamshidi, M. B. *et al.* Size reduction and performance improvement of a microstrip Wilkinson power divider using a hybrid design technique. *Nat. Scie. Rep.* **11**, 7773 (2021).
47. Qi, X. & Xiao, F. Filtering power amplifier with up to 4th harmonic suppression. *IEEE Access* **8**, 29021–29026 (2020).
48. Flattery, K. J., Amin, S., Mahamat, Y., Eroglu, A. & Ronnow, D. High power combiner/divider design for dual band RF power amplifiers. In *2015 International Conference on Electromagnetics in Advanced Applications (ICEAA), Turin, Italy*, 1036–1039 (2015).
49. Hayashi, H., Okazaki, H., Kanda, A., Hirota, T. & Muraguchi, M. Millimeter-wave-band amplifier and mixer MMICs using a broad-band 45/spl deg/ power divider/combiner. *IEEE Trans. Microw. Theory Tech.* **46**(6), 811–819 (1998).
50. Wang, E., Fu, X. & Tian, Q. Broadband power divider with phase shifter. In *2012 2nd International Conference on Consumer Electronics, Communications and Networks (CECNet), Yichang, China*, 1700–1702 (2012). https://doi.org/10.1109/CECNet.2012.6202069.
51. Golestanifar, A., Karimi, G. & Lalbakhsh, A. Varactor-tuned wideband band-pass filter for 5G NR frequency bands n77, n79 and 5G Wi-Fi. *Sci. Rep.* **12**, 16330. https://doi.org/10.1038/s41598-022-20593-x (2022).

Author contributions

G.M., S.S. and A.L. conceived the idea. G.M. and S.S. did the simulations and optimization. G.M, S.B, B.O, and A.L. developed the main idea for useable applications and designed the different structures. G.M. and S.B. did the theoretical analysis and proposed the circuit models. S.S., S.B., G.M., J.L.B. performed the measurements. G.M., S.S., A.L. and J.L.B. wrote and G.M., S.B., B.O., and J.L.B. edited the manuscript. All authors contributed to the discussion.

Competing interests

The authors declare no competing interests.

Additional information

Supplementary Information The online version contains supplementary material available at https://doi.org/10.1038/s41598-023-31019-7.

Correspondence and requests for materials should be addressed to A.L.

Reprints and permissions information is available at www.nature.com/reprints.

Publisher's note Springer Nature remains neutral with regard to jurisdictional claims in published maps and institutional affiliations.